# Primordial noble gas isotopes from immoderate crushing of an Icelandic basalt glass

R. Parai[1,2,*]

[1] Department of Earth and Planetary Sciences
Washington University in St. Louis, St. Louis, MO 63130

[2] McDonnell Center for the Space Sciences
Washington University in St. Louis, St. Louis, MO 63130

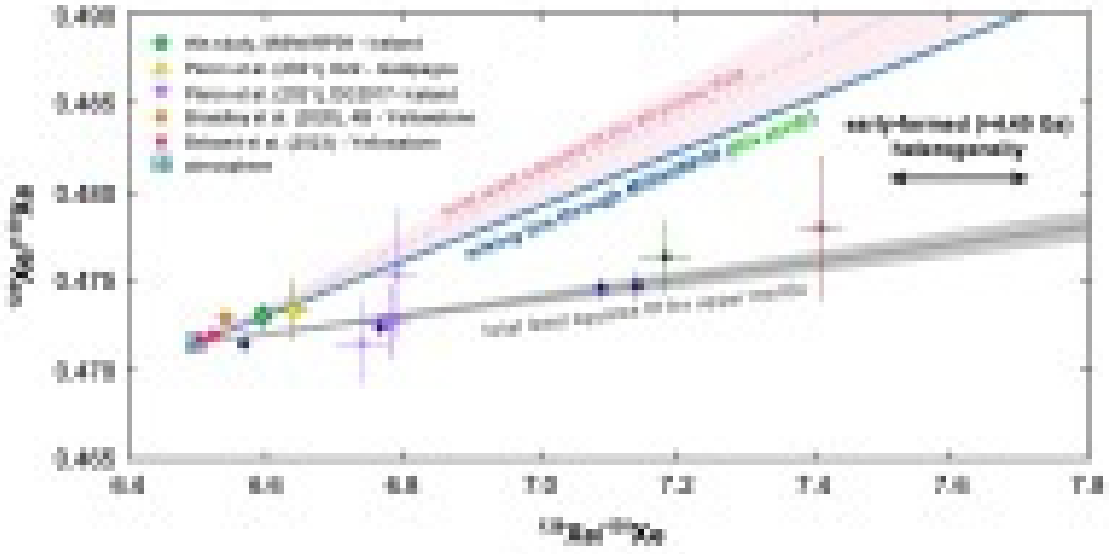

* Corresponding author (Email: parai@wustl.edu)

**Abstract**

Noble gas isotopes carry important information about volatile accretion, mantle differentiation and the preservation of early formed radiogenic isotope heterogeneities. However, extremely low abundances and pervasive atmospheric contamination make precise determinations of mantle source heavy noble gas isotopic compositions challenging. Furthermore, the precision achieved in ratios of the rarest noble gas isotopes (the primordial isotopes) is typically poor. Here an approach

that combines heavy crushing of a large quantity of sample along with more traditional temperate crushing is adopted to analyse noble gases in a basalt glass from Iceland. The method yields high precision Xe primordial isotope data resolved from the atmospheric composition. $^{128}Xe/^{130}Xe$–$^{129}Xe/^{130}Xe$ systematics indicate a distinct, low $^{129}Xe/^{130}Xe$ in the plume mantle source compared with that in the upper mantle, demonstrating the survival of an early formed (>4.45 Ga) radiogenic isotope heterogeneity in the modern mantle. Future sampling efforts may plan to dedicate large quantities (>20 g) of material for high precision noble gas analysis to leverage the advantages of a mixed analytical approach.

## Introduction

Precise determinations of mantle heavy noble gas (Ne, Ar, Kr and Xe) isotopic compositions have the power to shed light on the delivery of volatiles to Earth during accretion, and transport of volatiles among terrestrial reservoirs (*e.g.*, Parai and Mukhopadhyay, 2015; Péron and Moreira, 2018; Bekaert *et al*., 2019; Broadley *et al*., 2020; Péron *et al*., 2021). Two characteristics make the noble gases sensitive tracers of volatile transport: (1) due to their extremely low abundances in the solid Earth, production of specific isotopes by radioactive decay generates large radiogenic isotope signatures, even when the parent nuclide is itself rare, and (2) the noble gases tend to partition into gas phases when possible – that is, they broadly follow the major volatiles (such as water and carbon dioxide) and escape from the mantle to melts, and from lavas to the atmosphere, over time. These characteristics also make noble gases difficult to measure in volcanic rocks, especially in light of pervasive atmospheric contamination of volcanic rock samples (*e.g.*, Burnard *et al*., 1997; Ballentine and Barfod, 2000; Roubinet and Moreira, 2018). Analytical challenges have limited the

number and type of samples for which magmatic heavy noble gas isotopic ratios have been resolved from the atmospheric composition.

Various approaches have been adopted to battle atmospheric contamination and constrain mantle source noble gas isotopic compositions. Step release of gas from samples by crushing or heating has long been used to generate data arrays trending from the atmospheric isotopic signature towards a mantle composition (*e.g.*, Sarda *et al*., 1988; Marty, 1989); linear or hyperbolic mixing arrays can be used to determine a model mantle composition by assuming a solar-like mantle $^{20}Ne/^{22}Ne$ ratio (see Parai *et al*., 2019). Step release approaches have been used to determine mantle source $^{21}Ne/^{22}Ne$, $^{40}Ar/^{36}Ar$, and Xe isotopic compositions in mid-ocean ridge basalt and plume basalt samples. However, wide coverage of upper mantle and ocean island heterogeneity is yet to be achieved. Furthermore, mantle compositions for Kr and the rarest Xe isotopes ($^{124}Xe$, $^{126}Xe$, and $^{128}Xe$) are limited to unusually gas-rich basalt samples (Moreira *et al*., 1998), continental well gases (Caffee *et al*., 1999; Holland and Ballentine, 2006; Caracausi *et al*., 2016; Bekaert *et al*., 2019) and volcanic gases (Broadley *et al*., 2020; Bekaert *et al*., 2023), where large quantities of gas are available for analysis.

Recent studies have demonstrated the utility of a screening and accumulation method (Péron and Moreira, 2018) to achieve high precision measurements of rare noble gas isotopes (Péron *et al*., 2021). In this approach, gas from crush steps with $^{20}Ne/^{22}Ne$ above a certain threshold is progressively collected on a cold trap, and a large quantity of gas with a composition close to the mantle source is accumulated for Ar, Kr and Xe isotopic measurements (Péron and Moreira, 2018; Péron *et al*., 2021). This approach enables precise analysis of rare isotope ratios in accumulated gas with a reduced contribution from atmospheric contaminants. However, atmospheric contaminants may affect Ar, Kr and Xe isotopes in a given release step more strongly

than Ne isotopes due to high Ar/Ne, Kr/Ne and Xe/Ne ratios in the atmospheric contaminant compared to mantle gas. Thus, an accumulation approach using screening based on Ne isotopes may reduce but not eliminate atmospheric contamination in Ar, Kr and Xe. The trade off between the loss of information (*e.g.*, no mixing array from multiple gas release steps) and the gain in approaching the mantle composition using screened accumulation techniques must be weighed, and a hybrid approach may be best.

Another intuitive strategy to pursue precise measurements of rare noble gas isotopes in typical basalt samples is to crush heavily to release a very large amount of gas from a very large amount of sample in a single extraction step. However, the net benefit of this approach is unknown: in practice, the largest gas release steps tend to be close to atmospheric in composition, particularly in gas-poor basalts (Parai *et al*., 2012; Parai and Mukhopadhyay, 2015). By repeatedly crushing a sample in very small steps, one may generate (with less precise data) a well defined mixing array between atmosphere and the mantle composition, with some steps nearing a pure mantle composition (Mukhopadhyay, 2012; Parai and Mukhopadhyay, 2021). Very heavy crushing runs the risk of overwhelming small amounts of mantle gas with larger amounts of atmospheric gas in a single large gas release step, such that one obtains a very precise measurement of a nearly pure atmospheric contaminant rather than a good constraint on the mantle composition. However, this approach has not been tested in detail, potentially due to the risk it poses in making poor use of precious sample material.

Noble gas geochemistry is currently discussed in terms less specific ("plume mantle" *vs*. upper mantle) than the detailed discussions of mantle components in the broader mantle isotope geochemistry field. Radiogenic Sr, Nd, Pb and Hf isotopic co-variations among ocean island basalts shed light on multiple distinct compositional components within the plume mantle (*e.g.*,

HIMU, EM-I and EM-II; see Weis *et al*., 2023 for a recent review); the heavy noble gas isotopic signatures of these components remain to be determined. In order to bring valuable insights from heavy noble gases to bear on a wider array of mantle samples, it is critical to develop strategies that enable precise determinations of mantle source noble gas compositions in typical gas-poor volcanic samples. Here I report results from an experiment in which a hybrid crushing strategy was applied to a large quantity of Icelandic basalt glass. A few moderate crush steps were used to roughly calibrate subsequent gas release through several very large crush steps, with ~10–100× as much gas released *per* step than in prior studies that used a small step crush technique (Mukhopadhyay, 2012; Parai *et al*., 2012; Pető *et al*., 2013; Parai and Mukhopadhyay, 2015). While one cannot control the gas content of a given volcanic rock sample, very large amounts of sample can be collected for analysis using this heavy crushing method, unlocking new insights into heterogeneous volatile accretion and differentiation of the Earth's interior.

## Sample and Methods

Subglacial basalt glass was collected in the summer of 2009 from near Miðfell, Iceland (Supplementary Information). A large quantity of basalt glass rich in olivine crystals was collected from an outcrop of glassy pillow basalts by the eastern shore of Þingvallavatn off Route 36, near the location reported for the DICE sample (Harrison *et al*., 1999; Mukhopadhyay, 2012) and DG2017 (Péron *et al*., 2021).

He, Ne, Ar and Xe abundances and isotopic compositions were measured in the WUSTL Noble Gas Laboratory. Details of gas processing, mass spectrometry, and preparation of the gas standards are given in the Supplementary Information (Fig. S-2).

A mixed-size step crushing strategy was followed. Two small crush steps were used to roughly calibrate the expected $^{129}Xe$ signal as a function of the manometer reading. Steps 3–7 were "mega-crushes" targeting a $^{129}Xe$ signal ~50× higher than normally targeted in the laboratory (10,000 counts *per* second $^{129}Xe$ instead of 200 counts *per* second; see Supplementary Information for typical sensitivities) to enable precise measurement of the rarest Xe isotopes. None of the mega-crush steps required more than a single actuation of the hydraulic cylinder, which was slowly extruded while monitoring manometer pressure (in contrast to vigorous solenoid driven crushing). Once an audible change in the type of sound generated by crushing was noted (from cracks and pops to fainter crunches), the smaller crush method was resumed (Steps 8–13) to exhaust the gas supply in the sample. Xe blanks in the mass spectrometer were monitored after the large crushes to check for memory effects; no increase in the line blank was observed.

## Results and Discussion

He, Ne, Ar and Xe abundances and isotopic compositions from thirteen step crushes are reported in Supplementary Table S-1. Estimated $CO_2/^3He$, $^4He/^{21}Ne^*$, $^4He/^{40}Ar^*$ and other elemental abundance ratios are also given and are discussed in the Supplementary Information (Figs. S-3, S-4). The weighted average $^4He/^3He$ for the MiðfellRP09 sample is 41,200 ± 100 (1σ), in good agreement with prior studies of the DICE and DG2017 samples (Harrison *et al*., 1999; Mukhopadhyay, 2012; Péron *et al*., 2021). Ne, Ar and Xe isotopic compositions are shown in Figures 1–4.

***Mantle-atmosphere mixing systematics.*** Ne isotope ratio variations among the 13 individual crush steps are shown (Fig. 1) with the "mega-crush" gas release steps highlighted. The

mantle source $^{21}Ne/^{22}Ne_{(E)}$ calculated for mantle $^{20}Ne/^{22}Ne$ of 13.36 (solar nebular gas; Heber *et al.*, 2012) is 0.0373 ± 0.0003 (1σ; Fig. 1b), in good agreement with prior studies of Ne in DICE and DG2017 (Harrison *et al.*, 1999; Mukhopadhyay, 2012; Péron *et al.*, 2021). The first mega-crush step had the lowest measured $^{20}Ne/^{22}Ne$, corresponding to a large proportion of atmospheric contaminant in the measured gas, and over the course of five mega-crushes, the $^{20}Ne/^{22}Ne$ steadily increased (Fig. 1a).

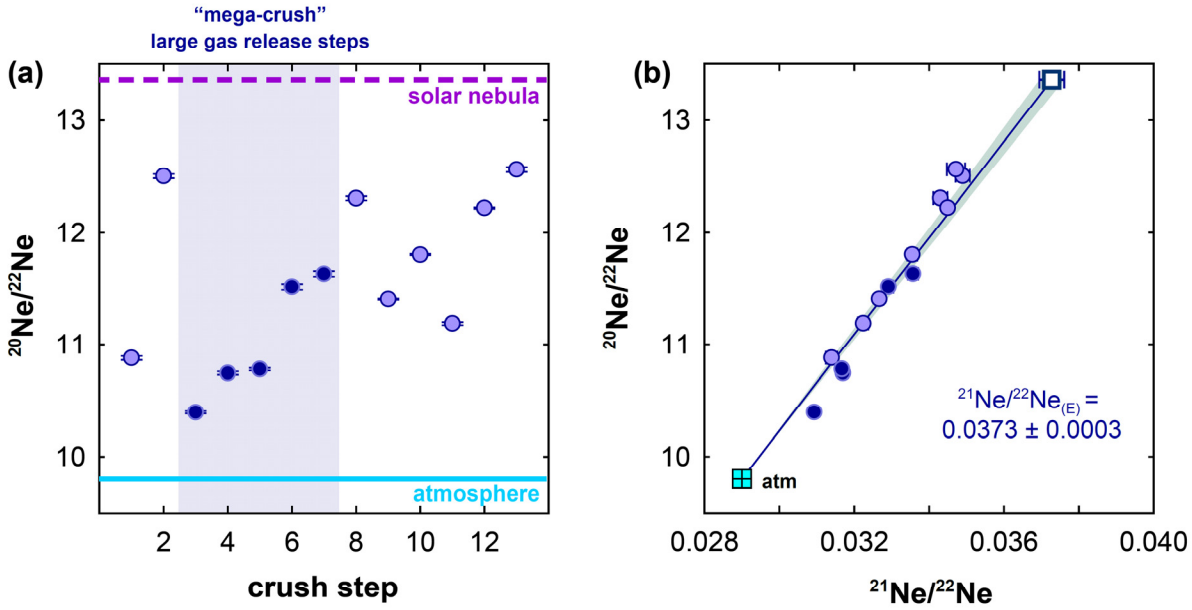


**Figure 1** Ne isotopes in MiðfellRP09 step crushes. $^{20}Ne/^{22}Ne$ is shown **(a)** as a function of crush step and **(b)** against $^{21}Ne/^{22}Ne$ (error bars 1σ). Dark circles represent the heavy crush steps, referred to as "mega-crush" steps. Ne in mega-crush steps starts off close to atmospheric, and progressively shifts towards mantle compositions. All crush steps taken together define a mixing line between atmosphere and an extrapolated mantle source $^{21}Ne/^{22}Ne$ of 0.0373 ± 0.0003 (1σ) assuming a solar-like mantle $^{20}Ne/^{22}Ne$ of 13.36.

Mixing between mantle and atmospheric compositions generates hyperbolic arrays in $^{20}Ne/^{22}Ne$ *vs*. $^{40}Ar/^{36}Ar$ space, reflecting distinct $^{36}Ar/^{22}Ne$ ratios in the mixing end members (Fig. 2). Ar/Ne and Xe/Ne ratios in the atmosphere and in air-saturated seawater are higher than those in mantle sources (Williams and Mukhopadhyay, 2019), and hyperbolic mixing arrays generated by step crushing thus have pronounced curvatures: addition of a small amount of atmospheric contaminant greatly affects Ar and Xe, without strongly affecting Ne (see Ne-Ar in Southwest Indian Ridge mid-ocean ridge basalt; Parai *et al*., 2012). The pronounced increase in $^{20}Ne/^{22}Ne$ in progressive mega-crush steps of the MiðfellRP09 sample is thus muted in $^{40}Ar/^{36}Ar$, $^{129}Xe/^{130}Xe$ and $^{129}Xe/^{132}Xe$, though the measured gas is still not totally overwhelmed by atmosphere.

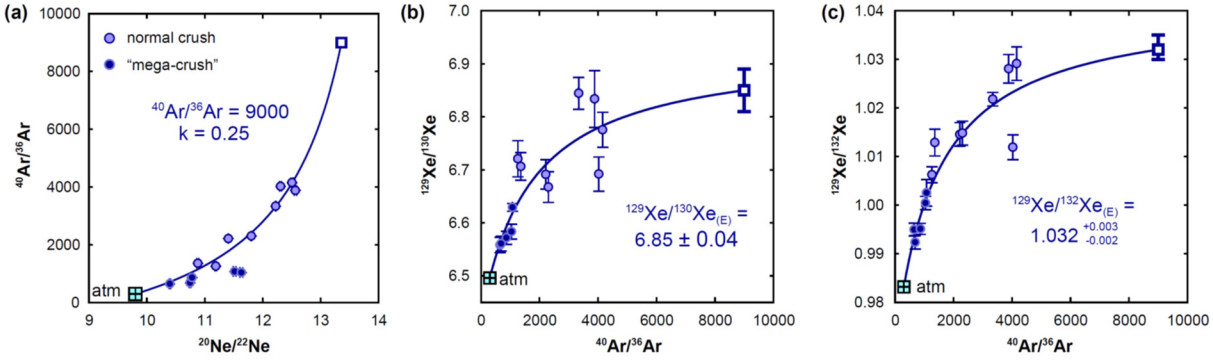


**Figure 2** Ne-Ar and Ar-Xe mixing systematics in MiðfellRP09 step crushes. Data are shown along with best fit two component mixing hyperbola determined by total least squares (error bars 1σ). **(a)** In $^{40}Ar/^{36}Ar$ *vs*. $^{20}Ne/^{22}Ne$, comparable fits can be achieved for a range of mantle end member $^{40}Ar/^{36}Ar$ ratios with compensating variation in the curvature parameter. Data and best fit mixing hyperbolae for $^{40}Ar/^{36}Ar$ *vs*. **(b)** $^{129}Xe/^{130}Xe$ and **(c)** $^{129}Xe/^{132}Xe$ are shown. In Ar-Xe, the

mega-crush step data are tightly clustered and constrain the mixing hyperbolae, though they are more affected by atmospheric contamination than the relatively scattered normal-sized crush step data.

Best fit mixing hyperbolae (Fig. 2) were determined by error weighted orthogonal least squares (Parai *et al*., 2012). The mantle source $^{40}Ar/^{36}Ar$ was not well resolved given the scatter in the data in Ne-Ar space (Fig. 2a) – good fits could be achieved with many pairings of mantle $^{40}Ar/^{36}Ar$ and curvature parameters (Fig. S-5). Applying a curvature parameter ($k$ = 0.25) consistent with the contrast between $^{36}Ar/^{22}Ne$ in the atmosphere and Iceland mantle source (Williams and Mukhopadhyay, 2019) yields a best mantle source $^{40}Ar/^{36}Ar$ of 9,000 (Fig. S-5). This mantle source $^{40}Ar/^{36}Ar$ was used to find best fit mantle source $^{129}Xe/^{130}Xe$ and $^{129}Xe/^{132}Xe$ (Fig. 2b,c). Given the concave down curvature of the mixing arrays in Ar-Xe space, the extrapolated mantle source Xe isotopic compositions are only weakly sensitive to the exact mantle source $^{40}Ar/^{36}Ar$. Despite having only 13 crush steps, the estimated mantle source Xe isotope compositions (Table S-2) are in excellent agreement with those determined using the 51 small crush steps in Mukhopadhyay (2012). However, the inclusion of a mix of small and mega-crush steps seems critical: the small crush steps provide a spread in compositions ranging towards mantle-like values, while the mega-crush steps provide precise measurements that are tightly clustered and define a mixing hyperbola (Fig. 2c).

The promising $^{129}Xe/^{130}Xe$ excesses compared to atmosphere in the mega-crush steps raise the question of whether $^{124}Xe/^{130}Xe$, $^{126}Xe/^{130}Xe$ and $^{128}Xe/^{130}Xe$ are also well resolved from atmosphere. In the small crush steps, the primordial Xe isotope ratios are highly uncertain and

scattered around the atmospheric composition (Fig. 3). In the mega-crush steps, primordial Xe isotope ratios are determined with much greater precision. $^{129}Xe/^{130}Xe$ is well resolved from atmosphere, while primordial isotope ratios either are not resolved (Fig. 3d) or show slight excesses (Fig. 3c,e) compared to atmosphere. The $^{129}Xe/^{130}Xe$ ratios are well resolved from atmosphere in part due to greater precision (Fig. S-2), but also due to the ~10× greater proportional difference between mantle source and atmospheric end member compositions in $^{129}Xe/^{130}Xe$ (~6.95 and 6.496, respectively) compared to the primordial isotope ratios (*e.g.*, $^{128}Xe/^{130}Xe$ of ~0.475 and 0.4715 in the mantle source and atmosphere, respectively).

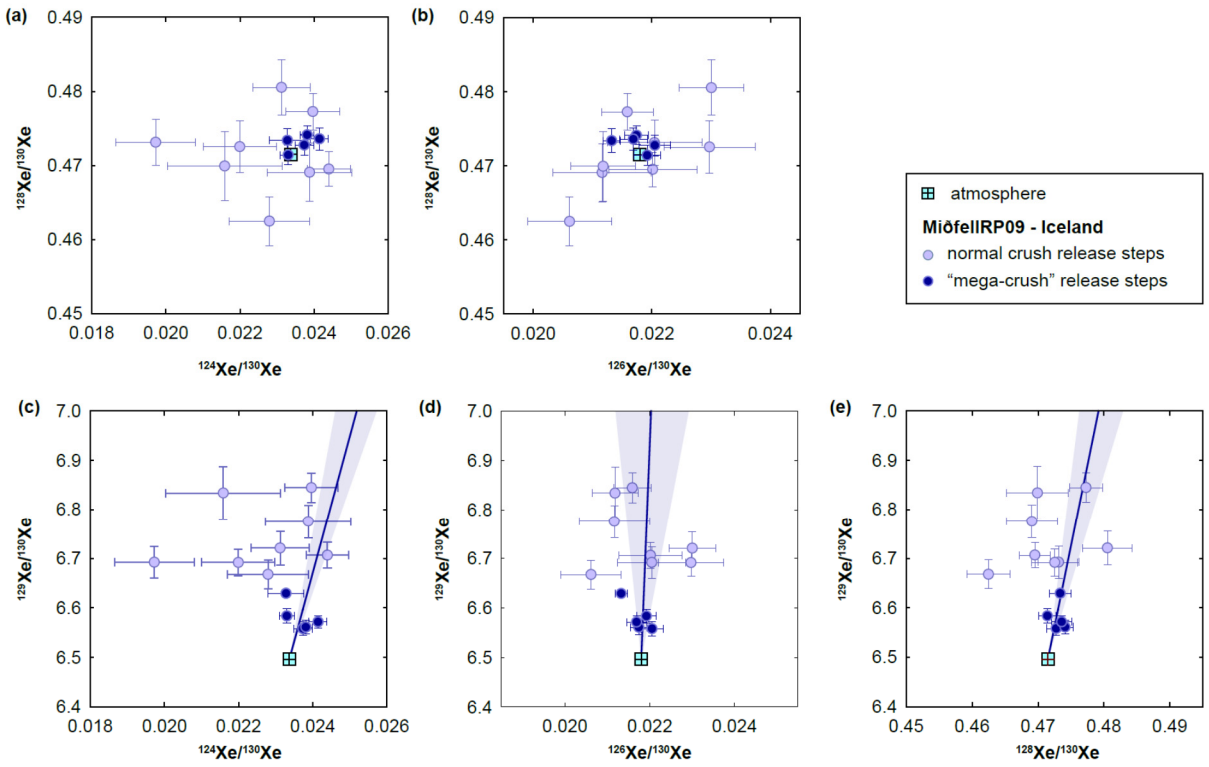


**Figure 3** Xe primordial isotopes and $^{129}Xe/^{130}Xe$. Data are shown with 1σ error bars. Among the normal crush steps, data are scattered with large error bars around the atmospheric composition.

The mega-crush step data include steps that are resolved from the atmospheric composition in **(a)** $^{124}Xe/^{130}Xe$ and $^{128}Xe/^{130}Xe$, though the relationship is not evident in **(b)** $^{128}Xe/^{130}Xe$ *vs*. $^{126}Xe/^{130}Xe$. $^{129}Xe/^{130}Xe$ is plotted against the primordial isotope ratios in panels **(c–e)** along with fits through atmosphere and the error weighted averages of mega-crush data.

***Early formed mantle heterogeneity in $^{129}Xe/^{130}Xe$.*** The improved precision and clear excess compared to atmosphere enable investigation of the nature of $^{129}Xe/^{130}Xe$ variations in the mantle. High $^{129}Xe/^{130}Xe$ in the mantle was generated by decay of short lived $^{129}I$ in the first ~100 Myr of Earth history, while high mantle $^{136}Xe/^{130}Xe$ was generated by a spontaneous fission of both short lived $^{244}Pu$ and extant $^{238}U$. By plotting $^{129}Xe/^{130}Xe$ against a ratio of two primordial isotopes, $^{3}He/^{130}Xe$, in the DICE sample (Iceland) and a North Atlantic mid-ocean ridge basalt, Mukhopadhyay (2012) argued for low $^{129}Xe/^{130}Xe$ in the mantle sources (corrected for atmospheric contamination) of plumes compared to the upper mantle, supported by additional data from mantle-derived samples with unfractionated elemental ratios (Pető *et al*., 2013; Parai and Mukhopadhyay, 2021). A similar comparison can be made using a ratio of two primordial Xe isotopes (*e.g.*, $^{128}Xe/^{130}Xe$) if precise, non-atmospheric data are available. Such a Xe three isotope plot has the advantage of being insensitive to whether elemental abundance ratios were fractionated by magmatic degassing (which does not generate resolvable Xe isotopic fractionation), meaning that Xe data from degassed samples may be included.

The error weighted average of MiðfellRP09 mega-crush steps gives a high precision determination of a trapped magmatic gas composition with clear excesses relative to atmosphere in $^{128}Xe/^{130}Xe$–$^{129}Xe/^{130}Xe$ space, and shows a distinct, steeper slope for Iceland compared to the

upper mantle (Fig. 4b; see Fig. S-6 for discussion of individual data sources). This translates to low $^{129}Xe/^{130}Xe$ in the plume mantle after accounting for atmospheric contributions (shallow contamination or regassing). The precise primordial isotope ratio ($^{128}Xe/^{130}Xe$) determined by mega-crushing thus confirms that the plume mantle had a low I/Xe ratio in the first 100 Myr of Earth history, and that early formed $^{129}Xe$ heterogeneity from $^{129}I$ decay has been preserved through 4.45 Gyr of mantle convection.

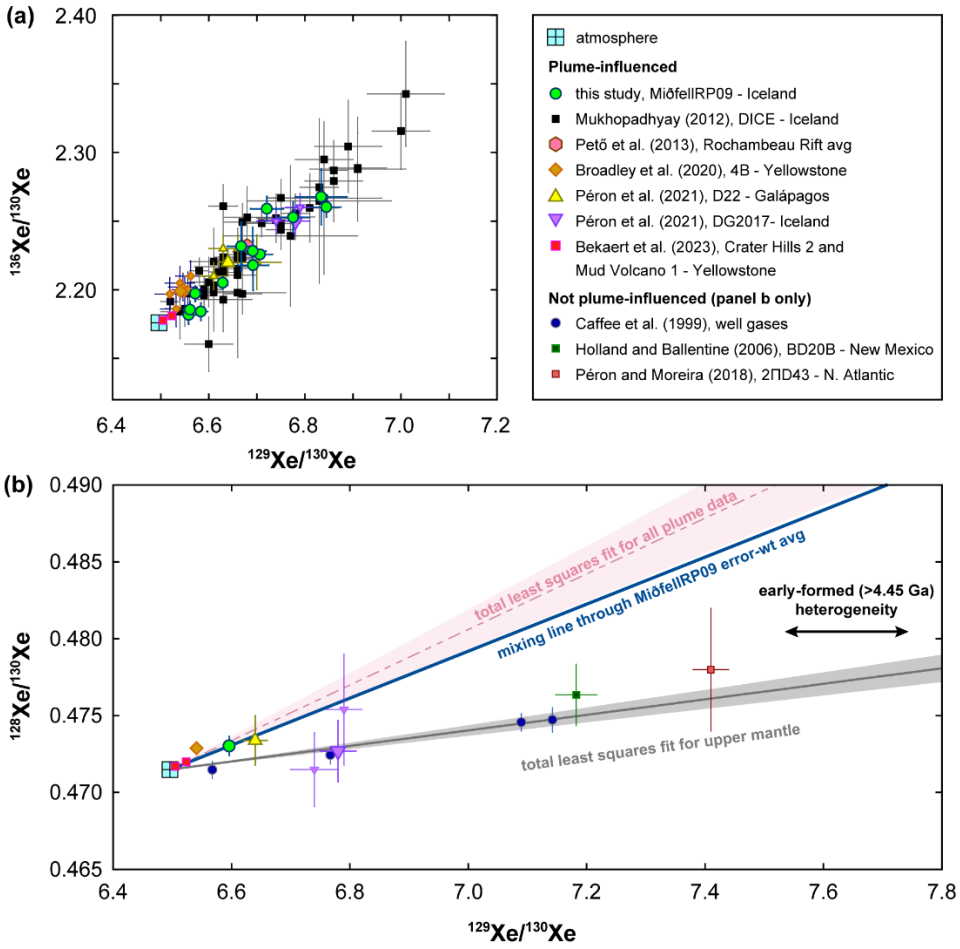


**Figure 4** MiðfellRP09 and literature Xe isotopic data. Small symbols are individual data, while larger symbols are averages. **(a)** Mega-crush and regular crush step $^{136}Xe/^{130}Xe$ *vs.*

$^{129}Xe/^{130}Xe$ data (1σ error bars) are consistent with prior Xe measurements in Iceland samples (Mukhopadhyay, 2012; Péron *et al*., 2021) and plume-influenced samples from Rochambeau Rift (Samoan plume), Galápagos, and Yellowstone (Pető *et al*., 2013; Broadley *et al*., 2020; Bekaert *et al*., 2023). **(b)** The error weighted average of mega-crush step $^{128}Xe/^{130}Xe$ *vs*. $^{129}Xe/^{130}Xe$ data (1σ error bars), along with average or most mantle-like compositions from plume and upper mantle samples (Péron and Moreira, 2018; Caffee *et al*., 1999; Holland and Ballentine, 2006; Bekaert *et al*., 2023; see Fig. S-6 for details). Fits forced through atmosphere and a mixing line between the MiðfellRP09 average and atmosphere are shown. The slope of the plume fit is strongly affected by the precisely determined Yellowstone 4B average, which may reflect some mass dependent fractionation in the hydrothermal system (Bekaert *et al*., 2023). While individual measurements for DG2017 (Péron *et al*., 2021) are shown, only the average was used to compute the best plume slope and its uncertainty. Despite a larger uncertainty in the plume fit, the plume and upper mantle fits have distinct slopes. The MiðfellRP09 mega-crush average is precisely determined, shows a prominent excess relative to atmosphere, and is consistent with data from other plume localities. The MiðfellRP09 average lies on a steeper slope than the upper mantle fit, indicating a plume mantle source with a lower $^{129}Xe/^{130}Xe$ at a given $^{128}Xe/^{130}Xe$ than the upper mantle.

## Conclusions

This study leveraged a new analytical method of heavy crushing of basalt glass to determine mantle source noble gas isotopic compositions. Precise determination of $^{128}Xe/^{130}Xe$–$^{129}Xe/^{130}Xe$ in MiðfellRP09 indicates that early formed $^{129}Xe/^{130}Xe$ heterogeneity persists in the mantle today. A hybrid analytical approach that leverages the advantages of different techniques may be the

optimal strategy for future work, but requires large quantities of material: likely >20 g of basalt glass *per* sample, perhaps more material for olivines. Future sampling efforts should incorporate this need in order to shed light on whether noble gas isotopic signatures of volatile origins, early differentiation and long term mantle outgassing vary among the full range of diverse mantle components sampled by oceanic basalts.

**Acknowledgments**

I am very grateful to David Graham and an anonymous reviewer for comments that improved the manuscript, and thank Anat Shahar for editorial handling. I thank Julian Rodriguez, Xinmu Zhang and Nathan Vaska for their vital assistance in the assembly, calibration and tuning of the gas extraction and purification line and mass spectrometer at Washington University. This work was supported by NSF EAR Petrology and Geochemistry grant 2145663 to RP.

**References**

Ballentine, C.J., Barfod, D.N. (2000) The origin of air-like noble gases in MORB and OIB. *Earth and Planetary Science Letters* 180, 39–48. https://doi.org/10.1016/S0012-821X(00)00161-8

Bekaert, D.V., Broadley, M.W., Caracausi, A., Marty, B. (2019) Novel insights into the degassing history of Earth's mantle from high precision noble gas analysis of magmatic gas. *Earth and Planetary Science Letters* 525, 115766. https://doi.org/10.1016/j.epsl.2019.115766

Bekaert, D.V., Barry, P.H., Broadley, M.W., Byrne, D.J., Marty, B., *et al*. (2023) Ultrahigh-precision noble gas isotope analyses reveal pervasive subsurface fractionation in hydrothermal systems. *Science Advances* 9, eadg2566. https://doi.org/10.1126/sciadv.adg2566

Broadley, M.W., Barry, P.H., Bekaert, D.V., Byrne, D.J., Caracausi, A., Ballentine, C.J., Marty, B. (2020) Identification of chondritic krypton and xenon in Yellowstone gases and the timing of terrestrial volatile accretion. *Proceedings of the National Academy of Sciences* 117, 13997–14004. https://doi.org/10.1073/pnas.2003907117

Burnard, P., Graham, D., Turner, G. (1997) Vesicle-Specific Noble Gas Analyses of "Popping Rock": Implications for Primordial Noble Gases in Earth. *Science* 276, 568–571. https://doi.org/10.1126/science.276.5312.568

290 Caffee, M.W., Hudson, G.B., Velsko, C., Huss, G.R., Alexander Jr., E.C., Chivas, A.R. (1999)
291 Primordial Noble Gases from Earth's Mantle: Identification of a Primitive Volatile Component.
292 *Science* 285, 2115–2118. https://doi.org/10.1126/science.285.5436.2115

293 Caracausi, A., Avice, G., Burnard, P.G., Füri, E., Marty, B. (2016) Chondritic xenon in the Earth's
294 mantle. *Nature* 533, 82–85. https://doi.org/10.1038/nature17434

295 Harrison, D., Burnard, P., Turner, G. (1999) Noble gas behaviour and composition in the mantle:
296 constraints from the Iceland Plume. *Earth and Planetary Science Letters* 171, 199–207.
297 https://doi.org/10.1016/S0012-821X(99)00143-0

298 Heber, V.S., Baur, H., Bochsler, P., McKeegan, K.D., Neugebauer, M., Reisenfeld, D.B., Wieler,
299 R., Wiens, R.C. (2012) Isotopic mass fractionation of solar wind: Evidence from fast and slow
300 solar wind collected by the *Genesis* mission. *The Astrophysical Journal* 759, 121.
301 https://doi.org/10.1088/0004-637X/759/2/121

302 Holland, G., Ballentine, C.J. (2006) Seawater subduction controls the heavy noble gas composition
303 of the mantle. *Nature* 441, 186–191. https://doi.org/10.1038/nature04761

304 Marty, B. (1989) Neon and xenon isotopes in MORB: implications for the earth-atmosphere
305 evolution. *Earth and Planetary Science Letters* 94, 45–56. https://doi.org/10.1016/0012-
306 821X(89)90082-4

307 Moreira, M., Kunz, J., Allègre, C. (1998) Rare Gas Systematics in Popping Rock: Isotopic and
308 Elemental Compositions in the Upper Mantle. *Science* 279, 1178–1181.
309 https://doi.org/10.1126/science.279.5354.1178

310 Mukhopadhyay, S. (2012) Early differentiation and volatile accretion recorded in deep-mantle
311 neon and xenon. *Nature* 486, 101–104. https://doi.org/10.1038/nature11141

312 Parai, R., Mukhopadhyay, S. (2015) The evolution of MORB and plume mantle volatile budgets:
313 Constraints from fission Xe isotopes in Southwest Indian Ridge basalts. *Geochemistry,*
314 *Geophysics, Geosystems* 16, 719–735. https://doi.org/10.1002/2014GC005566

315 Parai, R., Mukhopadhyay, S. (2021) Heavy noble gas signatures of the North Atlantic Popping
316 Rock 2ΠD43: Implications for mantle noble gas heterogeneity. *Geochimica et Cosmochimica*
317 *Acta* 294, 89–105. https://doi.org/10.1016/j.gca.2020.11.011

318 Parai, R., Mukhopadhyay, S., Standish, J.J. (2012) Heterogeneous upper mantle Ne, Ar and Xe
319 isotopic compositions and a possible Dupal noble gas signature recorded in basalts from the
320 Southwest Indian Ridge. *Earth and Planetary Science Letters* 359–360, 227–239.
321 https://doi.org/10.1016/j.epsl.2012.10.017

322 Parai, R., Mukhopadhyay, S., Tucker, J.M., Pető, M.K. (2019) The emerging portrait of an ancient,
323 heterogeneous and continuously evolving mantle plume source. *Lithos* 346–347, 105153.
324 https://doi.org/10.1016/j.lithos.2019.105153

Péron, S., Moreira, M. (2018) Onset of volatile recycling into the mantle determined by xenon anomalies. *Geochemical Perspectives Letters* 9, 21–25. https://doi.org/10.7185/geochemlet.1833

Péron, S., Mukhopadhyay, S., Kurz, M.D., Graham, D.W. (2021) Deep-mantle krypton reveals Earth's early accretion of carbonaceous matter. *Nature* 600, 462–467. https://doi.org/10.1038/s41586-021-04092-z

Pető, M.K., Mukhopadhyay, S., Kelley, K.A. (2013) Heterogeneities from the first 100 million years recorded in deep mantle noble gases from the Northern Lau Back-arc Basin. *Earth and Planetary Science Letters* 369–370, 13–23. https://doi.org/10.1016/j.epsl.2013.02.012

Roubinet, C., Moreira, M.A. (2018) Atmospheric noble gases in Mid-Ocean Ridge Basalts: Identification of atmospheric contamination processes. *Geochimica et Cosmochimica Acta* 222, 253–268. https://doi.org/10.1016/j.gca.2017.10.027

Sarda, P., Staudacher, T., Allègre, C.J. (1988) Neon isotopes in submarine basalts. *Earth and Planetary Science Letters* 91, 73–88. https://doi.org/10.1016/0012-821X(88)90152-5

Weis, D., Harpp, K.S., Harrison, L.N., Boyet, M., Chauvel, C., Farnetani, C.G., Finlayson, V.A., Lee, K.K., Parai, R., Shahar, A. (2023) Earth's mantle composition revealed by mantle plumes. Nature Reviews Earth & Environment, 4, 604–625. https://doi.org/10.1038/s43017-023-00467-0

Williams, C.D., Mukhopadhyay, S. (2019) Capture of nebular gases during Earth's accretion is preserved in deep-mantle neon. *Nature* 565, 78–81. https://doi.org/10.1038/s41586-018-0771-1

Geochemical Perspectives Letters


# Primordial noble gas isotopes from immoderate crushing of an Icelandic basalt glass

**R. Parai**

## Supplementary Information

The Supplementary Information includes:

- Sample Information
- Gas Extraction and Processing
- Mass Spectrometry Methods
- WUSTL House Gas Standards
- Elemental Ratios
- Supplementary Tables S-1 and S-2
- Supplementary Figures S-1 to S-6
- Supplementary Information References

## Sample Information

The MiðfellRP09 sample was collected by RP at 64°10'09.8"N, 21°03'27.5"W. While Harrison *et al.* (1999) report collection from a quarry 1 km east of the lake, the sample analysed in this study (Fig. S-1) was collected by the lake shore and adjacent to a small municipal waste collection area.


**Figure S-1** Pillow basalt and MiðfellRP09 glass. **(left)** Vesicular, olivine phenocryst-rich basalt, glass was abundant (1/4" cold chisel for scale). **(right)** Five pieces of glass over 10 g in mass were analysed in a single crusher chamber.

## Gas Extraction and Processing

Five pieces of vesicular glass weighing a total of 10.5627 g were cleaned in distilled water and acetone and then dried. The sample was loaded into a stainless steel cup with ultra-high vacuum aluminium foil liner, separated into three layers by tungsten carbide discs. The cup was loaded in a single large-geometry crusher chamber (see schematic of similar, smaller crusher chamber in Parai *et al*., 2009). Gases were released by step-crushing driven by a hand-pumped hydraulic cylinder while monitoring the pressure of released gas using an MKS capacitance manometer. An automated, compact, low-internal-volume gas extraction and processing line designed and built at WUSTL was used to prepare gases for analysis using the Nu Noblesse HR 5F5M noble gas mass spectrometer. Noble gases were purified by exposing the gas released by step-crushing to hot and cold SAES NP10 getters. A small aliquot (<1 % of total gas) was separated and analysed on a Stanford Research Systems residual gas analyser to estimate expected signals for He and Ar and to determine how to split the He and Ar prior to inlet to the mass spectrometer. Purified gas was exposed to a Janis cryotrap with a charcoal sorbent at 32 K, trapping noble gases heavier than He. Ne, Ar and Xe were sequentially released from the cryotrap and analysed separately.

## Mass Spectrometry Methods

Measurements were made using the Nu Noblesse HR 5F5M in the Department of Earth and Planetary Sciences at Washington University in St. Louis. The source trap current and filament voltage were optimised for Xe analysis and kept constant throughout all analyses, meaning that source tuning was suboptimal for He but was sufficient to make useful measurements -- reproducibility of $^{4}He/^{3}He$ in standards with similar amounts of gas as the sample were routinely <1 %. $^{3}He$ was measured on an electron multiplier fitted with a slit to enable resolution of $^{3}He^{+}$ from $HD^{+}$.

Ne was measured by multicollection in high mass resolving power mode, with $^{40}Ar^{++}$ resolved from $^{20}Ne^{+}$. $CO_2^{+}$ was monitored during the run by peak jumping, and a correction for $CO_2^{++}$ interference with $^{22}Ne$ was made using a $CO_2^{++}/CO_2^{+}$ was 0.01878 (following Parai *et al.*, 2009). The $CO_2^{++}/CO_2^{+}$ was determined by repeated calibrations using background $CO_2$ in the mass spectrometer at different $CO_2$ pressures, varied by partially closing the valve to the source getter pump. No relationship with total pressure was observed, consistent with prior studies (*e.g.*, Mukhopadhyay *et al.*, 2012). For mega-crush steps, $^{20}Ne$ was measured on a Faraday; for all other analyses, all Ne isotopes were measured on electron multipliers.

Ar was also measured by multicollection in high mass resolving power mode to enable resolution of hydrocarbon interferences from $^{38}Ar^{+}$. Chlorine backgrounds were monitored during the run by peak jumping. $HCl^{+}/Cl^{+}$ ratios were calibrated in the same manner as $CO_2^{++}/CO_2^{+}$, and corrections for $H^{35}Cl$ and $H^{37}Cl$ interferences were made using $HCl^{+}/Cl^{+}$ ratios of 0.17 and 0.18, respectively.

Xenon was measured in three steps, with masses 126, 128 and 130 on the axial mass in successive steps. Source tuning optimised sensitivity over mass resolving power as hydrocarbon interferences could be avoided even with low mass resolving power settings.

Instrument sensitivity, mass discrimination, and reproducibility were determined by repeat analyses of an in-house gas standard made by mixing a $^{3}He$-doped helium gas standard and dry air collected in Forest Park, St. Louis. Fifty-eight bracketing standards were run with 13 sample crush steps. Typical sensitivities were ~$3.5 \times 10^{6}$ V $^{4}He$ *per* ccSTP, $1.7 \times 10^{14}$ cps $^{20}Ne$ *per* ccSTP, ~$1.8 \times 10^{7}$ V $^{40}Ar$ *per* ccSTP, and $2.5 \times 10^{15}$ cps $^{129}Xe$ *per* ccSTP. The reproducibility of standards of similar size to crush steps was characterised to estimate uncertainties on measured values (Fig. S-2).

Blanks were determined by following the full procedure for a crush without actuating the hydraulic cylinder that would crush the sample. Blanks were <1 % for He, Ne and Ar for all crush steps. For Xe, blanks were <0.4 % for mega-crush steps, and <5 % for all other steps.

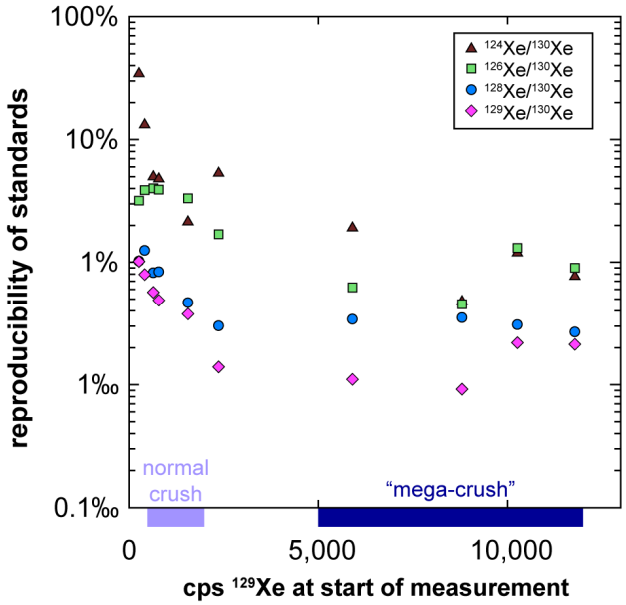


**Figure S-2** Reproducibility of standards as a function of signal size. Signal size is shown as counts *per* second of $^{129}$Xe at the start of the measurement. Reproducibility is the standard deviation in the isotope ratio measured in a set of standards of a given size divided by the mean isotope ratio for that set. Statistics are shown for $^{124}$Xe/$^{130}$Xe, $^{126}$Xe/$^{130}$Xe, $^{128}$Xe/$^{130}$Xe, and $^{129}$Xe/$^{130}$Xe. The reproducibility of standards at large signal sizes (for mega-crush steps) was 1–2 ‰ in $^{129}$Xe/$^{130}$Xe, and <1 % for the primordial Xe isotope ratios.

## WUSTL House Gas Standards

Two house gas standards were mixed in the WUSTL Noble Gas Laboratory. A house helium standard was mixed using a high purity $^{3}$He isotope spike purchased from Chemgas (Boulogne-Billancourt, France). A large (8 L) cylinder was prepared along with a helium standard mixing manifold with parts dedicated for the purpose of mixing a helium standard (Swagelok gasket-sealed bellows valves, standard conflat flange fittings, a VAT angle valve, two leak valves and two MKS Baratron capacitance manometers). The cylinder and manifold were rough pumped and all internal volumes were determined using pure nitrogen and MKS Baratron Absolute Pressure Sensors along with a calibrated volume. The system was baked, pumped for several days at ultra-high vacuum, sealed off and transported to a hallway. In this hallway, research-grade ultra-high purity He from Airgas was inlet through one leak valve to fill the 8 L cylinder and portions of the mixing manifold with He (mostly $^{4}$He), with the final pressure recorded using a manometer with a 10 torr max range. The $^{3}$He spike bottle was attached to the other leak valve and a small volume was filled to a pressure recorded using a manometer with a 0.1 torr max range. Target pressures for both filling steps were calculated to yield a mixture with mantle-like $^{4}$He/$^{3}$He. A valve separating the small volume filled with $^{3}$He and the rest of the mixing manifold and cylinder was opened and the system was left to equilibrate for an hour. A VAT all-metal right angle valve was used to seal off the 8 L cylinder, and the helium standard was named LHF, with a calculated $^{4}$He/$^{3}$He of 59,170. The rest of the manifold was pumped out in the hallway using a rough pump borrowed from another lab, and then put into storage.

Two 6 L standard tanks made by Achron Helium Systems (Austin, TX, USA) were prepared: they were pumped out, internal volumes were determined, they were baked and pumped for several days. One 6 L standard tank was attached to a filling manifold along with a ~5 cc volume filled with air collected in Forest Park, St. Louis during exceedingly dry conditions accompanying a polar vortex event in February

2021. The ~1 cc pipette volume of this 6 L tank was filled with a dose of polar vortex air, the outer valve was closed and the inner valve was opened to let the air equilibrate with the cylinder volume.

Both 6 L standard tanks were then attached to a small manifold along with the LHF cylinder. One aliquot from the LHF cylinder was used to fill the pipette volumes (~1 cc) of the two 6 L standard tanks. The outer pipette valves were closed, and the inner pipette valves were opened to let the LHF helium equilibrate with the cylinder volumes. Accordingly, one 6 L standard tank contains an LHF-doped polar vortex air standard named PVA, with $^4He/^3He$ of 59,240 and atmospheric Ne, Ar, Kr and Xe isotopic compositions. The other 6 L standard tanks contains LHF. Both standard tanks were installed on the WUSTL gas extraction and purification line.

## Elemental Ratios

A manometer directly attached to the crusher chamber was used to monitor pressure during gas release. The manometer records pressure during the crush and after the gas is expanded into a known volume. The drop in pressure is used to determine crusher volume for each crush step. Assuming the dominant species in the released gas is $CO_2$, moles of $CO_2$ can be calculated. The estimated $CO_2/^3He$ ratio is $1.3 \times 10^9$ (Fig. S-3), in excellent agreement with the value determined for DG2017 (Péron *et al*., 2021), and in broad agreement with measurements of DICE and other mantle samples (Marty and Tolstikhin, 1998; Marty *et al*., 2020).

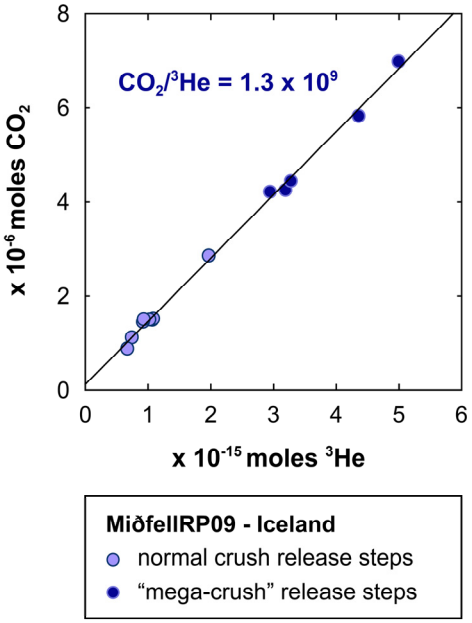


**Figure S-3** $CO_2$ *vs*. $^3He$ moles released in individual crush steps. $CO_2$ moles were estimated based on manometer readings and are an upper limit estimate assuming the main volatile species in the released gas was $CO_2$. There is a good correlation between the manometer pressure and moles of $^3He$. This correlation allowed for reliable targeting of "mega-crush" steps with a roughly predictable Xe signal.

The average $^4He/^{40}Ar^*$ ratio is 1.6 (Table S-1), on the low end of the range of estimated mantle production ratio, and the average $^4He/^{21}Ne^*$ is $1.7 \times 10^7$, low compared to the mantle production ratio (Yatsevich and Honda, 1997; Graham, 2002). These values are also lower than those measured in the DICE sample (Mukhopadhyay, 2012), indicating that elemental abundance ratios in the MiðfellRP09 sample have been affected by fractionation.

Plotting elemental ratios against isotopic ratios yields arrays that are rotated compared to DICE (Mukhopadhyay, 2012) in a systematic fashion consistent with kinetic fractionation driving preferential

loss of He compared to heavier noble gases. He-Ne and He-Ar systematics are illustrated in Figure S-4; element ratio-isotope ratio diagrams involving Xe are highly scattered.

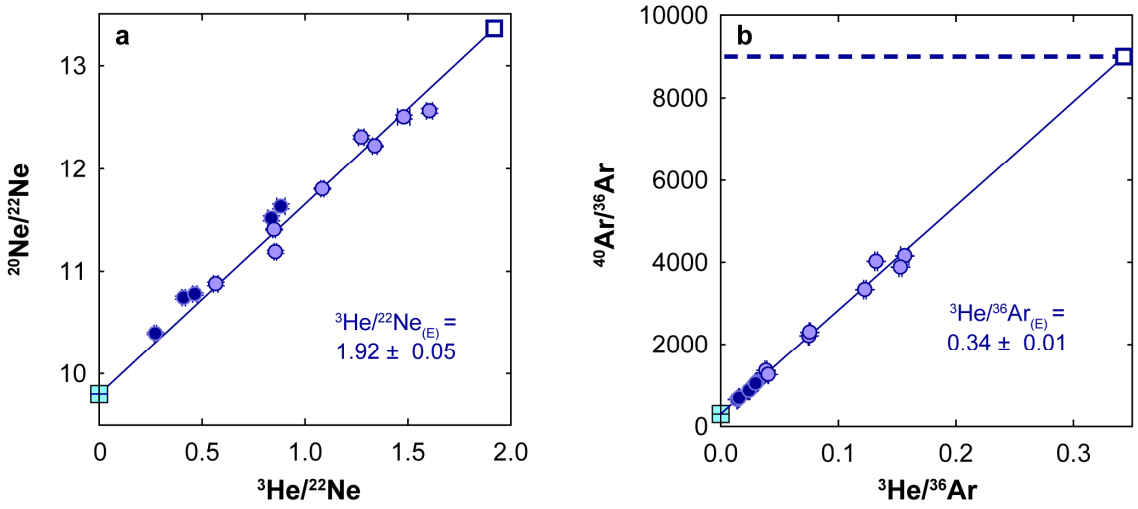


**Figure S-4** Elemental ratio *vs*. isotope ratio plots for MiðfellRP09 crush step data. Symbols as in Figure S-3. Good correlations are evident in **(a)** $^{20}Ne/^{22}Ne$ *vs*. $^{3}He/^{22}Ne$ and **(b)** $^{40}Ar/^{36}Ar$ *vs*. $^{3}He/^{36}Ar$. Extrapolated mantle source elemental ratios are given for a model mantle with $^{20}Ne/^{22}Ne$ = 13.36 (solar nebular gas), and $^{40}Ar/^{36}Ar$ of 9000. The resulting mantle $^{3}He/^{22}Ne$ and $^{3}He/^{36}Ar$ are low compared to mantle ratios estimated in studies of the DICE sample (Mukhopadhyay, 2012; $^{3}He/^{22}Ne$ of ~2.5 at the same $^{20}Ne/^{22}Ne$ and ~0.75 at the same $^{40}Ar/^{36}Ar$ as used here). The MiðfellRP09 $^{3}He/^{22}Ne$ and $^{3}He/^{36}Ar$ can be used to estimate a mantle $^{22}Ne/^{36}Ar$ of ~0.18, lower than estimated by Mukhopadhyay (2012), but similar to the value used by Williams and Mukhopadhyay (2019) for Iceland. All of the estimated mantle elemental ratios are depleted in the light element, consistent with kinetic fractionation effects and low $^{4}He/^{40}Ar^{*}$ and $^{4}He/^{21}Ne^{*}$ ratios.

## Supplementary Tables

**Table S-1** He, Ne, Ar, Xe and $CO_2$ abundances, He, Ne, Ar and Xe isotopic compositions and elemental abundance ratios in step-crush analyses of MiðfellRP09.

Table S-1 (.xlsx) is available for download from the online version of this article at https://doi.org/10.7185/geochemlet.2331.

**Table S-2** Mantle source isotope ratios determined using total least squares fits to air-mantle mixing models.

| | $^{21}Ne/^{22}Ne_{(E)}$ | $^{40}Ar/^{36}Ar_{(E)}$ | $^{129}Xe/^{130}Xe_{(E)}$ | $^{129}Xe/^{132}Xe_{(E)}$ |
|---|---|---|---|---|
| MiðfellRP09 | 0.0373 | 9000 | 6.85 | 1.032 |
| ±1σ | 0.0003 | (n/a)<br>See Figure S-5 | 0.04 | +0.003<br>−0.002 |

# Supplementary Figures

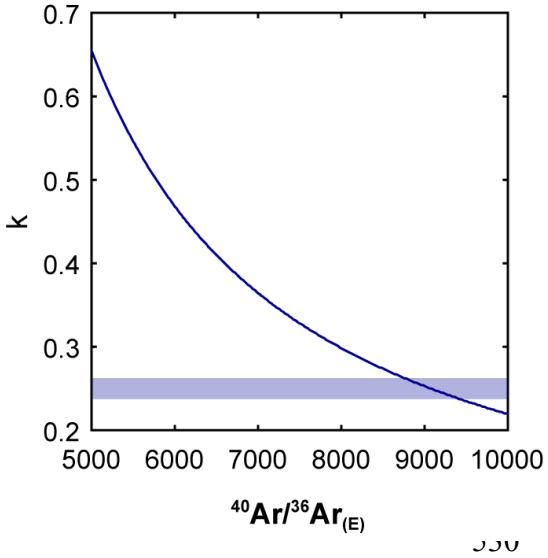


**Figure S-5** Best fit mantle $^{40}Ar/^{36}Ar_{(E)}$ as a function of hyperbolic mixing curvature parameter. Total least squares hyperbolic fitting using a mantle $^{20}Ne/^{22}Ne$ of 13.36 did not yield a well-resolved mantle source $^{40}Ar/^{36}Ar_{(E)}$ due to scatter in the data in Ne-Ar space (Fig. 2a). Fits with similar total scores could be achieved with many pairings of mantle $^{40}Ar/^{36}Ar$ and the curvature parameter $k$ (where $k$ values close to 1 approach linear mixing). The curve shows best pairings of these two parameters and illustrates how curvature can be strengthened to compensate for higher $^{40}Ar/^{36}Ar$. Applying a curvature parameter ($k$ = 0.25) consistent with the contrast between $^{36}Ar/^{22}Ne$ in the atmosphere and that estimated for the Iceland mantle source (Williams and Mukhopadhyay, 2019) yields a $^{40}Ar/^{36}Ar_{(E)}$ of ~9000, which is adopted for the Ar-Xe fits shown in Figure 2.

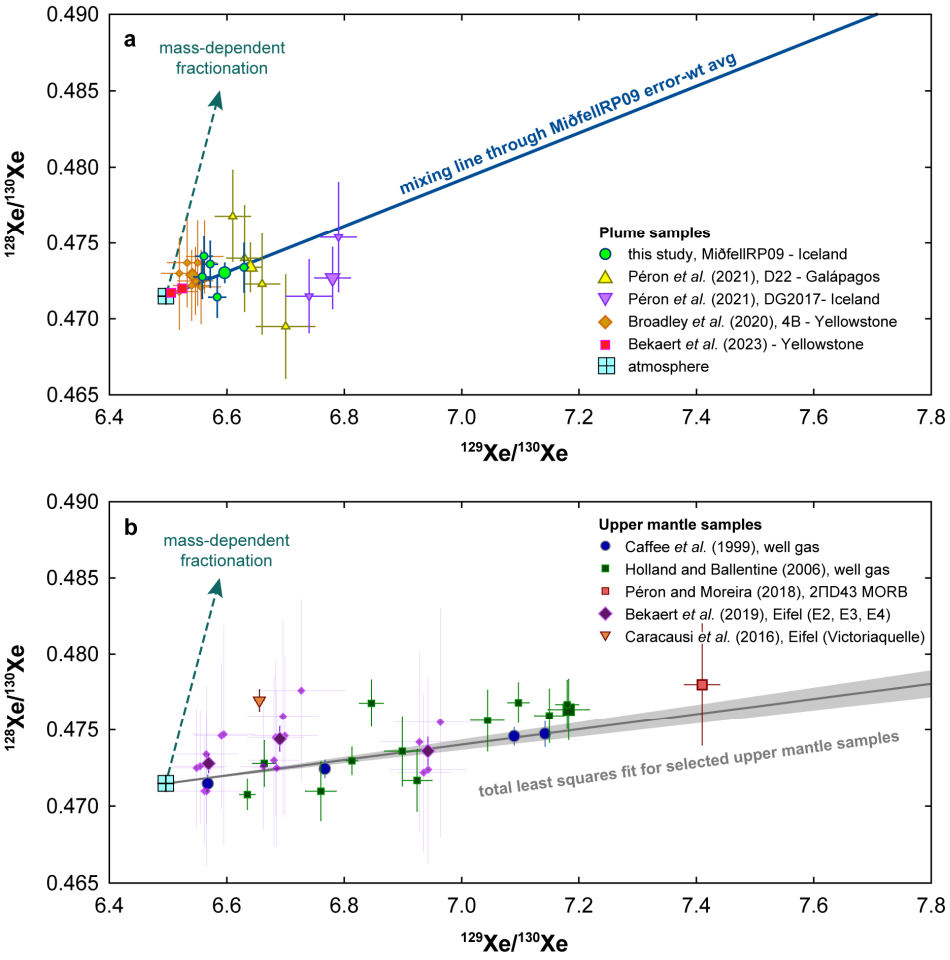


**Figure S-6** Individual and average $^{128}Xe/^{130}Xe$ *vs.* $^{129}Xe/^{130}Xe$ data for **(a)** plume and **(b)** upper mantle samples. For samples with differently sized symbols, the small symbols are individual measurements and large symbols are averages, except for the Bravo Dome well gas data from Holland and Ballentine (2006), where the large symbol shows the sample with least atmospheric contamination (BD20-B). The atmospheric composition and a mass-dependent fractionation trend through atmosphere are shown for reference. **(a)** Plume localities include Iceland (this study; Péron *et al.*, 2021), Galápagos (Péron *et al.*, 2021) and Yellowstone (Broadley *et al.*, 2020; Bekaert *et al.*, 2023). With very fine precision enabled by dynamic mass spectrometry, Bekaert *et al.* (2023) showed that volcanic gases are susceptible to mass-dependent fractionation due to diffusive transport within the hydrothermal system. Data from Bekaert *et al.* (2023) was screened using a plot of $^{128}Xe/^{130}Xe$ *vs.* $^{136}Xe/^{130}Xe$, which shows a population of samples dominated by mantle-atmosphere mixing and a population dominated by mass-fractionation. Among the samples dominated by mantle-atmosphere mixing, two with small $\delta^{86}Kr/^{84}Kr$ deviations from atmosphere are shown: Crater Hills 2 and Mud Volcano 1. The Yellowstone volcanic gas 4B average (Broadley *et al.*, 2020) is offset from the other Yellowstone measurements and may reflect a mass-dependent enrichment in light isotopes, but is included in the all-plume total least squares fit shown in Figure 4b. Galápagos data obtained using the screened accumulation technique (Péron *et al.*, 2021) is consistent with the MiðfellRP09 data from this study. One of the two individual measurements for Iceland (Péron *et al.*, 2021) agrees well with the other plume data, but the weighted average for Iceland-DG2017 is offset. **(b)** Upper mantle samples include well gases from Eifel (Caracausi *et al.*, 2016; Bekaert *et al.*, 2019), New Mexico, Colorado and

Australia (Caffee *et al.*, 1999; Holland and Ballentine, 2006), and a measurement of the N. Atlantic popping rock 2ΠD43 made using the screened accumulation technique (Péron and Moreira, 2018). Eifel data show indications of mass-dependent fractionation and are excluded from the upper mantle total least squares fit.

# Supplementary Information References


Bekaert, D.V., Broadley, M.W., Caracausi, A., Marty, B. (2019) Novel insights into the degassing history of Earth's mantle from high precision noble gas analysis of magmatic gas. *Earth and Planetary Science Letters* 525, 115766. https://doi.org/10.1016/j.epsl.2019.115766

Bekaert, D.V., Barry, P.H., Broadley, M.W., Byrne, D.J., Marty, B., *et al*. (2023) Ultrahigh-precision noble gas isotope analyses reveal pervasive subsurface fractionation in hydrothermal systems. *Science Advances* 9, eadg2566. https://doi.org/10.1126/sciadv.adg2566

Broadley, M.W., Barry, P.H., Bekaert, D.V., Byrne, D.J., Caracausi, A., Ballentine, C.J., Marty, B. (2020) Identification of chondritic krypton and xenon in Yellowstone gases and the timing of terrestrial volatile accretion. *Proceedings of the National Academy of Sciences* 117, 13997–14004. https://doi.org/10.1073/pnas.2003907117

Caffee, M.W., Hudson, G.B., Velsko, C., Huss, G.R., Alexander Jr., E.C., Chivas, A.R. (1999) Primordial Noble Gases from Earth's Mantle: Identification of a Primitive Volatile Component. *Science* 285, 2115–2118. https://doi.org/10.1126/science.285.5436.2115

Caracausi, A., Avice, G., Burnard, P.G., Füri, E., Marty, B. (2016) Chondritic xenon in the Earth's mantle. *Nature* 533, 82–85. https://doi.org/10.1038/nature17434

Graham, D.W. (2002) Noble Gas Isotope Geochemistry of Mid-Ocean Ridge and Ocean Island Basalts: Characterization of Mantle Source Reservoirs. *Reviews in Mineralogy and Geochemistry* 47, 247–317. https://doi.org/10.2138/rmg.2002.47.8

Harrison, D., Burnard, P., Turner, G. (1999) Noble gas behaviour and composition in the mantle: constraints from the Iceland Plume. *Earth and Planetary Science Letters* 171, 199–207. https://doi.org/10.1016/S0012-821X(99)00143-0

Holland, G., Ballentine, C.J. (2006) Seawater subduction controls the heavy noble gas composition of the mantle. *Nature* 441, 186–191. https://doi.org/10.1038/nature04761

Marty, B., Tolstikhin, I.N. (1998) $CO_2$ fluxes from mid-ocean ridges, arcs and plumes. *Chemical Geology* 145, 233–248. https://doi.org/10.1016/S0009-2541(97)00145-9

Marty, B., Almayrac, M., Barry, P.H., Bekaert, D.V., Broadley, M.W., Byrne, D.J., Ballentine, C.J., Caracausi, A. (2020) An evaluation of the C/N ratio of the mantle from natural $CO_2$-rich gas analysis: Geochemical and cosmochemical implications. *Earth and Planetary Science Letters* 551, 116574. https://doi.org/10.1016/j.epsl.2020.116574

Mukhopadhyay, S. (2012) Early differentiation and volatile accretion recorded in deep-mantle neon and xenon. *Nature* 486, 101–104. https://doi.org/10.1038/nature11141

Mukhopadhyay, S., Ackert Jr., R.P., Pope, A.E., Pollard, D., DeConto, R.M. (2012) Miocene to recent ice elevation variations from the interior of the West Antarctic ice sheet: Constraints from geologic observations, cosmogenic nuclides and ice sheet modeling. *Earth and Planetary Science Letters* 337–338, 243–251. https://doi.org/10.1016/j.epsl.2012.05.015

598 Parai, R., Mukhopadhyay, S., Lassiter, J.C. (2009) New constraints on the HIMU mantle from neon and
599 helium isotopic compositions of basalts from the Cook–Austral Islands. *Earth and Planetary Science*
600 *Letters* 277, 253–261. https://doi.org/10.1016/j.epsl.2008.10.014

601 Péron, S., Moreira, M. (2018) Onset of volatile recycling into the mantle determined by xenon anomalies.
602 *Geochemical Perspectives Letters* 9, 21–25. https://doi.org/10.7185/geochemlet.1833

603 Péron, S., Mukhopadhyay, S., Kurz, M.D., Graham, D.W. (2021) Deep-mantle krypton reveals Earth's
604 early accretion of carbonaceous matter. *Nature* 600, 462–467. https://doi.org/10.1038/s41586-021-
605 04092-z

606 Williams, C.D., Mukhopadhyay, S. (2019) Capture of nebular gases during Earth's accretion is preserved
607 in deep-mantle neon. *Nature* 565, 78–81. https://doi.org/10.1038/s41586-018-0771-1

608 Yatsevich, I., Honda, M. (1997) Production of nucleogenic neon in the Earth from natural radioactive
609 decay. *Journal of Geophysical Research: Solid Earth* 102, 10291–10298.
610 https://doi.org/10.1029/97JB00395

611